Observation of a Distributed Epitaxial Oxide in Thermally Grown SiO_2 on Si(001)

A. Munkholm and S. Brennan
Stanford Synchrotron Radiation Laboratory, Stanford Linear Accelerator Center, Stanford, California 94309

F. Comin and L. Ortega
European Synchrotron Radiation Facility, B.P. 220, F-38043, Grenoble, France
(Received 8 May 1995; revised manuscript received 11 September 1995)

We present direct evidence of an ordered oxide which is epitaxially related to the underlying Si(001) substrate and is distributed throughout thermally grown oxide films with thicknesses between 80 and 1000 Å. This evidence consists of diffraction peaks at the $\langle 1, 1, 0.45 \rangle$ positions. For films with thickness in the range 80–160 Å the integrated intensity of these diffraction peaks increases roughly linearly and the ordered oxide grain size parallel to the surface is constant at 130 Å.

PACS numbers: 68.55.Jk, 61.10.Eq, 81.65.Mq

Oxidation of silicon has been a topic of considerable interest for both fundamental and technological reasons. The transition from perfect crystallinity in the substrate to the amorphous oxide is abrupt, yet there are few unbonded silicon atoms at the interface [1]. Technological development has achieved a density of interfacial dangling bonds of less than 1 per 10^5 atoms and a transition region from perfect crystallinity to seemingly pure amorphous material in less than 10 Å. However, the specific nature of the transition from the crystallinity of the substrate to the amorphous oxide film has been difficult to determine, due to its buried nature and the inherently challenging problem of characterizing the decay of long-range order.

After the prediction of a boundary layer of microcrystallites [2] for a thermally grown oxide a number of groups reported observation of these features, using both transmission electron microscopy [3,4] and grazing incidence x-ray scattering [5]. More recently, epitaxial interfacial oxides have been seen on native and room-temperature dry and wet oxides as well [6–8]. Until now, however, there has been no direct evidence of a ordered oxide distributed throughout a thermally grown oxide film.

For the past decade the termination of bulk order has been studied using crystal truncation rod (CTR) scattering [9,10]. The CTR is an excess of scattered intensity away from a bulk Bragg peak in the direction of the surface. It is by modulation of CTR scattering that indirect evidence of a distributed epitaxial oxide has been seen [11]. In this Letter, we report direct evidence of an epitaxial ordered oxide which is present throughout thermally grown oxides of thicknesses 80, 115, 160, and 1000 Å. In addition to observing the modulation of the CTR scattering, the period of which corresponds to the film thickness in each case, we have observed scattering from the ordered oxide responsible for the modulation of the CTR. The integrated intensity of the ordered oxide peak increases roughly linearly with film thickness between 80 and 160 Å, but the integrated intensity from the 1000 Å film is only slightly larger than that of the 160 Å film, which may be a result of different processing conditions. The increase in ordered oxide integrated intensity with thickness coupled with the period of the oscillations in the CTR scattering is conclusive evidence that the oxide is not limited to the interface, as has been seen previously, but is distributed throughout the oxide film.

The samples used in these experiments are commercially produced 6 in. Si(001) wafers. The 80 Å oxide was grown using a dry oxide process. The 115 and 160 Å oxides were produced using a wet-dry process. The 1000 Å oxide was grown using a steam process. The substrates are typically within 0.1 deg of the (001) orientation.

Experiments were performed at both the Stanford Synchrotron Radiation Laboratory (SSRL) and at the European Synchrotron Radiation Facility (ESRF). At SSRL the experiments were performed on beam line 7-2 with a four-circle diffractometer using a symmetric scattering geometry ($\omega = 0$ mode). The energy of the photons was selected to be 10.1 keV by a Si(111) double crystal monochromator. The scattering from the ordered peak was mapped out by both radial scans and rocking curves for all samples. For our purposes radial scans increase the scattering vector length parallel to the surface ($h = k$) without changing the out-of-plane length (l). Rocking curve (θ rotation) scans rotate the scattering vector with respect to reciprocal space without a change in length. The interference between the ordered peak and the CTR was detected both with an l scan (a scan through reciprocal space perpendicular to the surface) and with radial scans which sliced through the CTR at various perpendicular momentum transfers.

At the ESRF an ultrahigh vacuum surface diffractometer [12] was used to study the 1000 Å oxide sample, but for our experiments the vacuum was sufficient only to eliminate air scattering near the sample. Photons of 10.36 keV monochromated by a Si(111) double crystal monochromator were produced by the ID32 undulator. Both the horizontal and vertical divergence of this insertion device are very low (43 and 24 μrad), which result in

 0031-9007/95/75(23)/4254(4)$06.00 © 1995 The American Physical Society

very high scattering resolution, even without a diffracted beam analyzer crystal, as can be seen in Fig. 1. Similar radial and rocking curve scans to those at SSRL were taken to map out the ordered peak.

Figure 1(a) shows the scattering taken at ESRF along the CTR between the (110) surface peak and the (111) bulk reflection (l scan) for the 1000 Å oxide sample. Plotted is the region between $(1,1,0.35)$ and $(1,1,0.55)$. Here and elsewhere in this Letter we will be discussing positions or sizes in reciprocal space. In all cases the dimensions are in units of $2\pi/a_{\mathrm{Si}}$, i.e., 1.157 $\mathrm{Å}^{-1}$, where a_{Si} is the silicon unit cell dimension. Note that these data

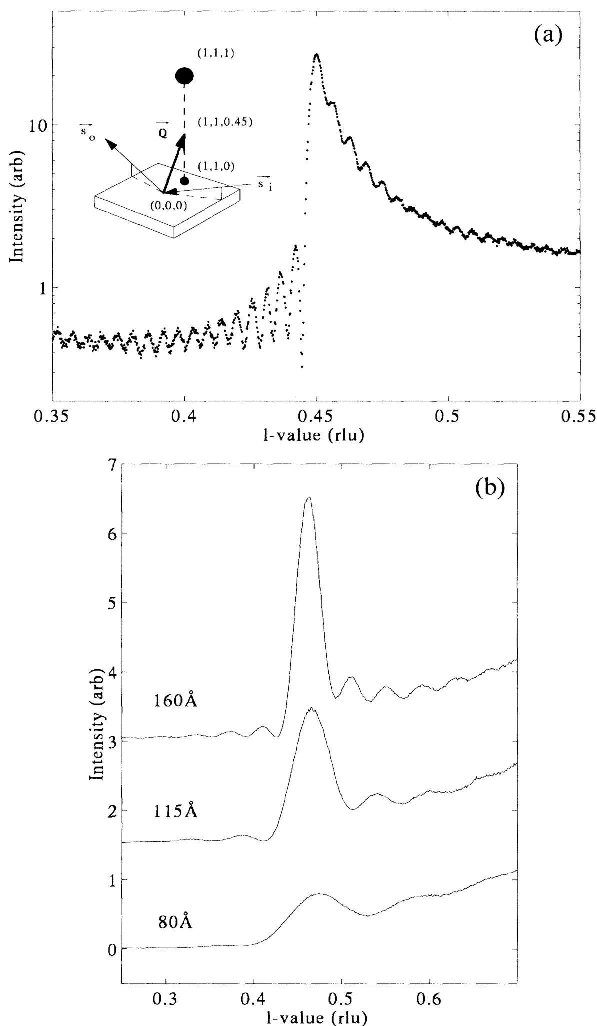

FIG. 1. (a) Scan of a 1000 Å thermally oxidized Si(001) wafer between 1, 1, 0.35 and 1, 1, 0.55. The oscillations in reciprocal space have the same periodicity as the thickness of the oxide film. The inset shows the portion of reciprocal space where the scattering is observed. The data were taken by scanning in the direction of the dashed line of the inset. (b) Scans similar to that of (a) for 80, 115, and 160 Å thermal oxide films from $(1,1,0.25)$ to $(1,1,0.70)$.

are plotted on a log scale, so that the jump in intensity at $l = 0.45$ is almost a factor of 85. The oscillations seen in the data have a periodicity which matches the 1000 Å oxide film thickness. Figure 1(b) is a set of three l scans for the 80, 115, and 160 Å samples. In this case the scanning range is from $(1,1,0.25)$ to $(1,1,0.70)$. The data are plotted on a linear scale, with an offset between scans for clarity. In all four curves of Fig. 1 the period (λ) of the oscillations in reciprocal space is related to the thickness (t) of the corresponding film by $t = a_{\mathrm{Si}}/\lambda$. The data shown in Fig. 1 were taken in an off-specular scattering geometry, i.e., the scattering vector is not aligned with the surface normal, so these oscillations are not due to Kiessig fringes such as are seen in low angle specular reflectivity of thin films. This can be seen in the diagram inset in Fig. 1(a), which shows the scattering geometry. Kiessig fringes would be observed along the $00l$ direction, whereas this scattering is seen between the $(1,1,0)$ and the $(1,1,1)$ positions. We are convinced that this effect is not due to simultaneous diffraction of multiple reflections from within the silicon crystal, because the scattering is observed at the same hkl with a variety of photon energies, e.g., 8.05, 10.1, and 10.53 keV.

To explore the scattering further, we have performed scans where $h = k$ at constant l in the vicinity of $(1,1,0.45)$, which are shown for the 160 Å oxide film in Fig. 2. This figure plots the log of the scattered intensity in a "waterfall" plot for a series of $h = k$ scans through $(1,1,l)$ with l values between 0.44 and 0.5. The central sharp peaks which these scans cut through make up the rod of scattering seen in Fig. 1(b), top. The thickness oscillations seen in that figure are also observable here. Figure 2 clearly shows an additional broad scattering peak which coincides with the scattering from the bulk silicon rod at $(1,1,0.45)$. It is this peak which we are convinced

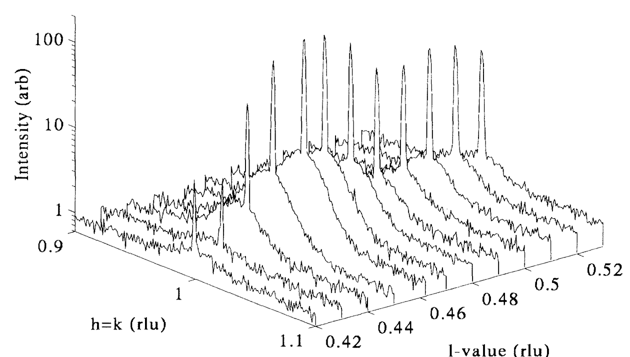

FIG. 2. Scans with $h = k$ near $(1,1,0.45)$ through the peak of the 160 Å thermal oxide sample seen in Fig. 1(b). These scans show not only the narrow strong scattering of Fig. 1 but also the broad weak scattering of an epitaxial ordered oxide which coincides with the bulk scattering.

is due to an ordered oxide within the amorphous thermal oxide film.

The scattering seen in Figs. 1 and 2 has been observed at all four of the $\langle 1,1,0.45\rangle$ positions. The peak position corresponds to scattering from planes with a periodicity of 3.66 Å. The limited width of the ordered oxide peaks ($\approx$0.5 deg wide for the 1000 Å film) in the h and k directions indicates that the oxide is well oriented with respect to the silicon substrate. Randomly oriented crystallites would result in a spherical shell of scattering at a scattering magnitude ($\sqrt{h^2 + k^2 + l^2}$) equal to that of the $(1,1,0.45)$. Note that the peak intensity of the oxide scattering (60 counts/sec) is a factor of 20 weaker than the intensity of the rod. In addition, the scattering from the rod at $(1,1,0.45)$ is more than 6 orders of magnitude weaker than the intensity of the bulk $(1,1,1)$ Bragg reflection. Thus the crystallinity of the oxide would be very difficult to observe without an intense synchrotron source. Although Si-SiO_2 is one of the most studied systems, the weak scattering explains why the ordering has not been observed using other techniques.

Rocking curves were performed through the maximum of the ordered oxide peak at $(1,1,0.45)$ for each of the four samples. The results are shown in Fig. 3. The integrated intensity was determined for each of these curves after removing the background and the CTR component. Normalized to the 80 Å sample, the ratio of the integrated intensity between the 80, 115, and 160 Å samples are given by 1, 2.70, and 3.53, respectively. The inset in Fig. 3 is a plot of the integrated intensity versus film thickness for these three samples, along with a best fit line through the data which also passes through $(0,0)$. The monotonic increase in ordered oxide intensity with film thickness is further evidence that the ordered oxide is distributed throughout the bulk of the film rather than situated at the interface. The 1000 Å oxide has an integrated intensity only slightly larger (4.01) than that of the 160 Å sample. We believe the deviations from linearity are due to differences in the processing procedures during their fabrication.

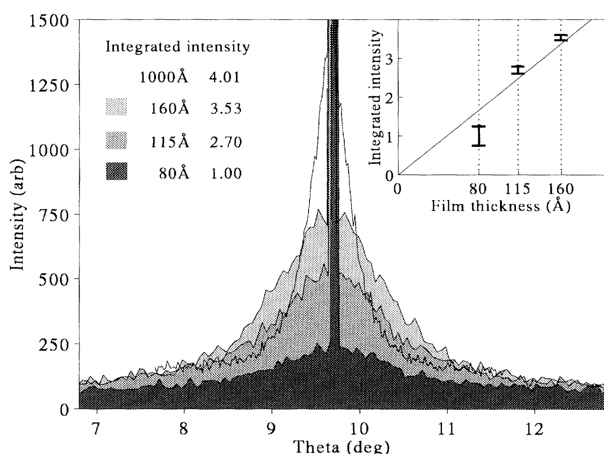

FIG. 3. Rocking curves through the maximum of the ordered oxide peak for the four oxide film thicknesses. The narrow strong feature in the center is the CTR scattering from the silicon substrate. In the inset table, the integrated intensities of the rocking curves have been normalized to that from the 80 Å oxide sample. The second inset shows the integrated intensity for the thinner oxide samples as a function of film thickness along with a best linear fit through $(0,0)$.

One can learn about the grain size of the ordered oxide perpendicular to the growth direction by radial and rocking scans at constant out-of-plane momentum transfer. The width of a rocking curve has contributions from mosaic spread, finite crystal size, and instrumental resolution. A radial scan width includes contributions from finite crystal size, instrumental resolution, and inhomogeneous strain. Differences in widths for the sample measured at ESRF and SSRL are due to differences in instrumental resolution. With the assumption that the instrumental broadening at ESRF is negligible, we can deconvolute the instrumental broadening at SSRL from the other effects. This assumption is justified by the small horizontal and vertical beam divergence of the ID32 undulator beam at ESRF.

Results of the analysis of crystallite size for the four film thicknesses are shown in Table I for both radial ($h = k$ at constant l) and rocking scans. The peak width (w) in reciprocal lattice units (rlu's) is related to the crystallite size in angstroms by $size = a_{\mathrm{Si}}/w$. The difference in rocking curve width between the ESRF and SSRL data is sufficiently small that it has no impact on the integrated intensity values quoted above. There is a significant difference in the measured width of the radial scan for the 1000 Å data, being 0.024 rlu's at SSRL and 0.009 rlu's at ESRF. The deconvolution factor derived from the 1000 Å sample was then applied to the thinner samples. For all samples the deconvoluted widths derived from the radial and rocking scans are equal to each other. Given that the width

TABLE I. Ordered oxide crystallite size for different thermal oxide film thicknesses. The maximum of the diffraction peak near $(1,1,0.45)$ has been scanned both in the radial direction ($h = k$ at constant l) and by a θ-rocking curve, such that the magnitude of the scattering vector is unchanged.

Film thickness (Å)	Scan type	Crystal Size (Å)
80	Rocking	128
80	Radial	130
115	Rocking	133
115	Radial	133
160	Rocking	138
160	Radial	132
1000	Rocking	407
1000	Radial	411

extracted from the radial scan involved a significant deconvolution whereas the width from the rocking curve involved almost no correction, this agreement is reassuring, and suggests that the domains of ordered oxide are cylindrically shaped. We conclude from these results that the broadening caused by inhomogeneous strain (for the radial scan) and that caused by mosaic spread (for the rocking curve) are small compared to the finite crystal size effect. For the three thinner samples both radial and rocking scans result in crystallite sizes of ~130 Å. The 1000 Å sample has a significantly larger grain size of ~410 Å. The grain size in the growth direction is extracted from the width of the oscillation in the l direction, and is equal to the film thickness in each case.

In conclusion, we have obtained direct evidence of an epitaxial ordered oxide distributed throughout thermally grown oxide films on Si(001) ranging in thickness from 80 to 1000 Å. The existence of a distributed ordered oxide was predicted by Takahashi, Shimura, and Harada [11] as a result of their observation of oscillations in the scattered intensity of the $11l$ rod. We observe these same oscillations and have also observed directly the scattering from the epitaxial oxide which is the cause of these oscillations. The integrated intensity of this oxide peak increases roughly linearly for similar oxidation processes, which demonstrates that the ordered oxide extends through the amorphous oxide film. The narrowness of the ordered oxide rocking curve indicates that these columnar grains are well oriented with respect to the substrate. The grain size in the plane perpendicular to the growth direction is constant for the thinner films (130 Å), but is significantly larger $\approx 3x$ for the 1000 Å film (410 Å). This suggests that the oxide ordering increases with film thickness, although changes in processing parameters are likely to play a significant role as well. We have looked for higher order diffraction peaks without success, thus making the derivation of the crystal structure difficult. The lack of higher order reflections suggests that the "crystallinity" of the ordered oxide is rather poor, with large amounts of static disorder. This perhaps explains why transmission electron micrographs have not observed these grains, which would otherwise be large enough to be seen. Given the weakness of the scattering from the ordered oxide peak, the concentration of this ordered oxide is probably below 1% of the total oxide film.

Part of this work was supported by SSRL, which is funded by the Department of Energy, Office of Basic Energy Sciences under Contract No. DE-AC03-76SF00515. The authors would like to thank A. Bienenstock for many valuable discussions and G. Renaud for assistance during the experiments at ESRF.

[1] N.F. Mott, S. Rigo, F. Rochet, and A.M. Stoneham, Philos. Mag. B **60**, 189 (1989).
[2] W.A. Tiller, J. Electrochem. Soc. **128**, 3 (1981); **130**, 689 (1983).
[3] R. Rochet, S. Rigo, M. Froment, C. d'Anterroches, C. Maillot, H. Roulet, and G. Dufour, Adv. Phys. **35**, 237 (1986).
[4] A. Ourmazd, D.W. Taylor, J.A. Tentschler, and J. Bevk, Phys. Rev. Lett. **59**, 213 (1987).
[5] P.H. Fuoss, L.J. Norton, S. Brennan, and A. Fischer-Colbrie, Phys. Rev. Lett. **60**, 600 (1988).
[6] G. Renaud, P.H. Fuoss, J. Bevk, B.S. Freer, and P.O. Hahn, Appl. Phys. Lett. **58**, 1044 (1991).
[7] T.A. Rabedeau, I.M. Tidswell, P.S. Pershan, J. Bevk, and B.S. Freer, Appl. Phys. Lett. **59**, 3422 (1991).
[8] T.A. Rabedeau, I.M. Tidswell, P.S. Pershan, J. Bevk, and B.S. Freer, Appl. Phys. Lett. **59**, 6 (1991).
[9] S.R. Andrews and R.A. Cowley, Solid State Phys. **18**, 6427 (1985).
[10] I.K. Robinson, Phys. Rev. B **33**, 3830 (1986).
[11] I. Takahashi, T. Shimura, and J. Harada, J. Phys. Condens. Matter **5**, 6525 (1993), and references therein.
[12] G. Renaud, B. Villette, and P. Guenard, Nucl. Instrum. Methods B **95**, 422 (1995).